2013 European Control Conference (ECC)
July 17-19, 2013, Zürich, Switzerland.

Automatic control of tethered wings for airborne wind energy: design and experimental results

L. Fagiano*, A. U. Zgraggen, M. Khammash and M. Morari

***Abstract*— A new approach to control tethered wings for airborne wind energy is described. A fixed length of the lines is considered, and the aim of the control system is to obtain figure-eight crosswind trajectories. The proposed technique is based on the notion of the wing's "velocity angle" and, in contrast with most existing approaches, it does not require a measurement of the wind speed or of the effective wind at the wing's location. Moreover, the proposed approach features few parameters, whose effects on the system's behavior are very intuitive, hence simplifying tuning procedures. Experimental results are presented, obtained by extensively testing the approach with a small-scale prototype.**

I. Introduction

Airborne wind is a new concept of renewable energy technology, whose aim is to convert the power of wind blowing up to 1000 m above the ground into electricity (see e.g. [1], [2], [3], [4], [5], [6], [7], [8], [9], [10], as well as [11] for an overview). In order to reach the target altitude, airborne wind energy generators employ tethered wings flying fast in crosswind conditions, i.e. roughly perpendicular to the wind flow [12]. The aerodynamic forces generated by the wing during its flight are large enough to keep the device in the air and to produce a significant amount of power.

Controls is one of the most important aspects of airborne wind generators. These devices have different operating phases, with corresponding different control objectives. In one of such phases, named *traction phase* [11], the aim is to make the wing fly along figure-eight paths in crosswind conditions: this kind of trajectories yields the highest traction forces on the lines, hence maximizing the produced power. The related control problem involves fast, nonlinear, unstable time-varying dynamics subject to hard operational constraints and external disturbances. Most of the approaches presented in the literature to tackle this problem are based on a nonlinear point-mass model of the system, derived on the basis of first-principle laws of mechanics and aerodynamics, and they involve the use of advanced nonlinear control design techniques, [6], [7], [8], [13], [14]. However, there are very few works in the literature, presenting a control system that has been actually tested in real-world experiments. One of such contributions is concerned with the control of large kites for seagoing vessels [15], and it employs a much simpler control-oriented model, justified by means of measured data. It has to be noted that a similar model has been considered also in [10], where it has been justified by a priori assumptions. The control approach proposed in [15] is composed by an inner control loop that computes the steering input needed to obtain a desired reference heading of the wing, and an outer control loop that computes the reference heading according to a bang-bang-like strategy. The inner control loop is a quite sophisticated model-following approach that needs the measure of the effective wind speed at the wing's altitude, obtained from an onboard anemometer.

We describe here a recently proposed control design approach for tethered wings [16], [17], whose aim is to achieve figure-eight crosswind paths. Differently from [7], [13], [10], the approach does not use pre-computed paths based on a model of the system, thus avoiding issues related to model mismatch and to the actual feasibility of the employed reference path for the (uncertain and time-varying) dynamics of a real system. Moreover, an estimate or measure of the wind speed at the wing's location, as considered in [6], [7], [13], is not needed in our approach, nor is a measure of the effective wind speed aligned with the wing longitudinal body axis, used in [15], but only a rough estimate of the wind direction with respect to the ground. The structure of the controller is similar to the one proposed in [15], but the design approach is different. In particular, the inner controller is a simple static gain plus a feedforward action, while the outer one is given by a switching strategy based on the wing's position. The proposed control approach involves few parameters that can be tuned in a very intuitive way. We present the experimental results obtained by extensive testing with a small-scale prototype realized at the University of California, Santa Barbara.

II. System description and model equations

A. System layout

We consider a flexible wing, or power kite, connected by three lines to a ground unit (GU), see Fig. 1. In normal flight conditions, the wing's trajectory evolves downwind with respect to the GU. For simplicity, we assume that the nominal wind direction (i.e. neglecting turbulence and small, zero-mean deviations) is aligned with the longitudinal symmetry axis of the GU, denoted by X. This condition can be achieved by properly orienting the GU, exploiting a measure or estimate of the nominal wind direction. With this assumption in mind, our control approach employs the feedback of the wing's position relative to the GU to obtain crosswind figure eight trajectories, i.e. flying paths that are downwind and symmetric with respect to X axis (i.e. the wind direction). The X axis, together with the Z axis being perpendicular to the ground and pointing upwards and with the Y axis to complete a right-handed system, forms the inertial frame $G \doteq (X, Y, Z)$, centered at the GU (see Fig. 2). By considering a fixed length of the lines, denoted by r, the wing's trajectory is thus confined on a quarter sphere,

978-3-952-41734-8/©2013 EUCA

Fig. 1. Small-scale prototype built at the University of California, Santa Barbara, to study the control of tethered wings for airborne wind energy.

given by the intersection of a sphere or radius r centered at the GU's location and the planes $(x, y, z) \in \mathbb{R}^3 : x \geq 0$ and $(x, y, z) \in \mathbb{R}^3 : z \geq 0$. Such a region is commonly named "wind window", see Fig. 2 (dashed lines).

The two lateral lines linking the wing to the GU, named steering lines, are attached to the back tips of the wing (see Fig. 1) and they are used to influence its trajectory: a shorter left steering line with respect to the right one impresses a left turn to the wing (i.e. a counter-clockwise turn as seen from the GU), and vice-versa. The center line, named power line, splits into two lines connected to the front of the wing (or leading edge) and sustains about 70% of the generated load. In the considered prototype, a single motor, together with a linear motion system (visible in the lower-left corner of Fig. 1), is able to change the difference of length of the steering lines. In this work, we consider a fixed length of the lines of $r = 30\,\text{m}$ and we focus on the problem of designing a controller able to make the wing fly along "figure-eight" crosswind paths, which maximize the generated forces.

The wing is equipped with inertial onboard sensors and a radio transmitter; the receiver and other sensors are installed on the GU, including a line angle measurement system, load cells, and an anemometer. The available sensors, together with suitable filtering algorithms, provide real-time measurements of the wing's position and velocity, to be used for feedback control, see [18], [19] for details. In the next sections, we introduce the notion of velocity angle of the wing and a control-oriented model that we will use for control design. Moreover, we give more details on the

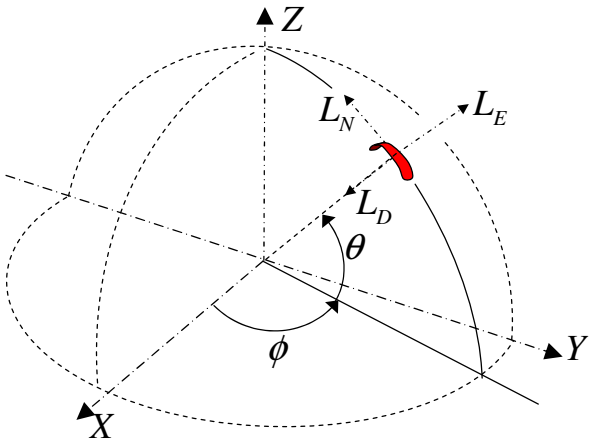

Fig. 2. Reference system $G = (X, Y, Z)$, wind window (dashed lines), variables θ, ϕ, and local north, east and down (L_N, L_E, L_D) axes.

specific geometry of the actuation system of our GU, which gives rise to a measurable additive disturbance acting on the control input. The latter, in turns, justifies the use of a feed-forward contribution in our controller.

B. Control-oriented model for tethered wings

Previous works in the literature employ a nonlinear point-mass model for control design, leading to multi-variable approaches (see e.g. [7], [8], [20] and the references therein). Here, we employ a simpler, single-input, single-output dynamical model to design one of the inner control loops in our approach. The model is based on the notion of the wing's velocity angle, which we will now introduce. By considering the fixed line length r, the wing's position $\vec{p}(t)$ can be expressed in the inertial frame G using the spherical coordinates $\theta(t)$, $\phi(t)$ (see Fig. 2), where t is the continuous time variable.

Let us consider a non-inertial coordinate system, $L \doteq (L_N, L_E, L_D)$, centered at the wing's position (depicted in Fig. 2). The L_N axis, or local north, is tangent to the sphere of radius r, on which the wing's trajectory evolves, and points towards its zenith. The L_D axis, called local down, points the center of the sphere (i.e. the GU), hence it is perpendicular to the tangent plane to the sphere at the wing's location. The L_E axis, named local east, forms a right hand system and spans the tangent plane together with L_N. We note that the system L is a function of the wing's position only, and it is different from the local systems used in previous works (see e.g. [8] and the references therein), due to the different definition for angle θ. The wing velocity vector, $\vec{v}(t) \doteq \frac{d}{dt}\vec{p}(t)$, can be expressed in the L frame as

$$ {}_L\vec{v} = \begin{pmatrix} r\dot{\theta} \\ r\cos(\theta)\dot{\phi} \\ 0 \end{pmatrix}. \tag{1} $$

Then, the velocity angle $\gamma(t)$ of the wing is defined as:

$$ \gamma(t) \doteq \arctan\left(\frac{\vec{v}\cdot\vec{e}_{L_E}}{\vec{v}\cdot\vec{e}_{L_N}}\right) = \arctan\left(\frac{\cos(\theta(t))\dot{\phi}}{\dot{\theta}}\right), \tag{2} $$

where $\vec{e}_{L_N}$, $\vec{e}_{L_E}$ are the unit vectors parallel to the L_N and L_E axes, respectively. The angle $\gamma(t)$ is thus the angle between the local north $L_N(t)$ and the wing velocity vector, $\vec{v}(t)$. This variable is particularly suited for feedback control, since it describes the flight conditions of the wing with just one scalar. In (2), the four-quadrant version of the arc tangent function shall be used, such that $\gamma \in [-\pi, \pi]$.

In [15] and [10], a variable similar to γ has been used, and a simple model has been proposed for the control design, of the following form:

$$\dot{\gamma}(t) \simeq \tilde{K}(t)\,\delta(t) + \tilde{T}(t), \tag{3}$$

where $\delta(t)$ is the steering input acting on the wing and $\tilde{K}(t)$, $\tilde{T}(t)$ are uncertain, time-varying parameters. Such a model has been justified mainly through experimental results in [15], where the gain $\tilde{K}(t)$ has been derived empirically, while in [10] it is the consequence of some assumptions. Equation (3) is indeed a model well-suited for control design, with the right balance between accuracy and simplicity, however neither [15] nor [10] provided a clear relationship between the model's parameters and the main characteristics of the system, such as wing size, mass, or efficiency. The theoretical result we recall next is aimed to fill this gap, by linking the model (3) to the first-principle models like the one used in [8].

Proposition 1: Let the wing fly in crosswind conditions, and assume small control inputs. Then, equation (3) holds with:

$$\tilde{K}(t) = \frac{\rho\, C_L(t)\, A\, |v_P(t)|}{2 m d_s} \left(1 + \frac{1}{E_{eq}^2(t)}\right)^2 \tag{4a}$$

$$\tilde{T}(t) = \frac{g \cos\left(\theta(t)\right) \sin\left(\gamma(t)\right)}{|v_P(t)|} + \sin\left(\theta(t)\right) \dot{\phi}(t), \tag{4b}$$

where ρ is the air density, A is the wing effective area, m is the ing mass, g is the gravity acceleration, $|v_P(t)|$ is the magnitude of the wing's velocity projected onto the plane (L_N, L_E), $E_{eq}(t) \doteq C_L(t)/C_{D,eq}(t)$, finally $C_L(t)$, $C_{D,eq}(t)$ are the wing's lift coefficient and the equivalent drag coefficient, respectively.

Proof: See [17]. ∎

In Proposition 1, the equivalent drag coefficient takes into account both the aerodynamic drag of the wing and the drag induced by the lines. Proposition 1 provides a simple and explicit link between the main lumped parameters of the wing, like area, mass and lift coefficient, and the gain $\tilde{K}(t)$ and external disturbance $\tilde{T}(t)$ of (3). See [17] for insights on the implications of this result.

C. Geometric steering input

The prototype used for our test flights features two attachment points for the steering lines on the GU, left and right. These attachment points are separated by a distance d (see Fig. 1, in the lower part, where the attachment points given by swaying pulleys are visible). This distance induces an equivalent steering deviation that we call "geometric input", δ_{g}, since its value depends on the geometry of the attachment points and on the (θ, ϕ) position of the wing in the wind window. Hence, the overall steering input acting on the wing is:

$$\delta(t) = \delta_{\mathrm{u}}(t) + \delta_{\mathrm{g}}(t), \tag{5}$$

where δ_{u} is the input issued by the control system, i.e.

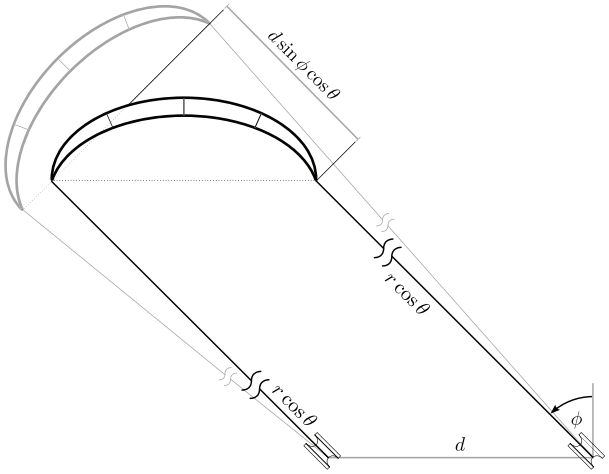

Fig. 3. Sketch of the wing in a generic (θ, ϕ) position as seen from above, and related geometric input $\delta_g = d\,\sin(\phi)\,\cos(\theta)$.

the difference of length of the steering lines obtained by changing the position of the linear motion system on the GU. In the following, we derive an expression to compute the geometric input as a function of $\theta(t)$, $\phi(t)$ and d. Consider the GU and the wing as seen from above, such that the trace of the wind window is a semicircle of radius $r\cos(\theta)$ and, for fixed θ, the wing position is univocally identified by ϕ. Let us consider first a situation in which both wing tips lie in the tangent plane to the wind window at the current wing position (θ, ϕ) (i.e. they lie on the tangent line to the circle of radius $r\cos(\theta)$ in our top view). Since the steering of the wing is essentially induced by a roll motion, by which the wing tips are moved away from the tangent plane, we call this orientation a neutral flying position (see Fig. 3, gray drawing). Now, assuming that $\delta_{\mathrm{u}} = 0$, the left and right lines have the same length, so that the wing tips are forced to leave the neutral flying position (see Fig. 3, black drawing), in the same way as a steering input were acting on the wing. In other words, in order for the wing to be in a neutral position in the presence of a value of $\phi \neq 0$, the two steering lines should have a difference of length equal to

$$\delta_{\mathrm{g}} = -d\,\sin(\phi)\cos(\theta). \tag{6}$$

We note that the geometric input is always bounded by d, moreover with an increasing θ position of the wing its value decreases and becomes eventually zero if the wing is at the zenith position of the wind window. The minus sign in (6) derives from the fact that the geometric input imposes a counter-clockwise turn (as seen from the GU) for $\phi < 0$ (i.e. $\dot{\gamma} > 0$, compare equations (3) and (5)) and a clockwise turn for $\phi > 0$ (i.e. $\dot{\gamma} < 0$).

III. CONTROL DESIGN

We employ a control scheme consisting of three nested loops, shown in Fig. 4. The outer control loop employs the current wing position, in terms of θ, ϕ angles, to compute a reference velocity angle, γ_{ref}, for the middle control loop. The latter exploits the γ as feedback variable and it has

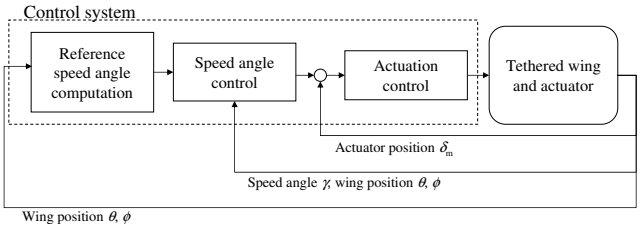

Fig. 4. Scheme of the overall proposed control system.

the objective of tracking γ_{ref}, by setting a suitable position reference, $\delta_{\text{m,ref}}$, for the actuator installed on the GU. The innermost control loop then employs a feedback of the motor position δ_{m} to command the motor's current i_{m}, in order to track the desired position $\delta_{\text{m,ref}}$. This control structure allows to separate the nonlinear part of the controller, which is all kept at the outermost level, from the linear one, hence obtaining two simple controllers for the middle and inner loops, for which we can carry out a theoretical robustness analysis. The values of θ, ϕ and γ can be measured or accurately estimated with the sensors available in our prototype [19]. We briefly describe next the main features of each control loop, for details the interested reader is referred to [17].

A. Position control loop

The innermost loop is a position control system with an electrical DC brushed motor and a linear motion system based on a lead screw mechanism. The feedback variable is the actuator's position in m, $\delta_{\text{m}}(t)$, measured with high accuracy by an optical rotary incremental encoder installed on the motor and suitably scaled to obtain the linear position of the actuator from the motor shaft's angular position, and the control input is the commanded motor's current, $i_{\text{m}}(t)$. Then, the GU is equipped with a series of pulleys such that, for a given value of δ_{m}, the corresponding difference of length of the steering lines is equal to

$$\delta_{\text{u}} = K_{\delta_{\text{u}}}\, \delta_{\text{m}}, \tag{7}$$

with some fixed gain $K_{\delta_{\text{u}}}$ (see section IV for the actual numerical values of our experimental setup). We use standard loop-shaping control design techniques (see e.g. [21]) to design a cascade feedback controller for the motor.

B. Velocity angle control loop

The control design for the middle loop exploits the control-oriented model (4) recalled in section II-B. The controlled variable is the velocity angle γ, and the control input is the actuator position $\delta_{\text{m,ref}}(t)$ (i.e. the target for the innermost control loop described in section III-A). The control objective is to track the desired velocity angle, γ_{ref}, issued by the outermost controller. The controller is given by a simple proportional law, plus a feedforward contribution based on the geometric input δ_{g} (6):

$$\delta_{\text{m,ref}}(t) = K_{\text{c}}\left(\gamma_{\text{ref}} - \gamma(t)\right) - K_{\text{f}}\delta_{\text{g}}(t), \tag{8}$$

where $\gamma_{\text{ref}}(t)$ is the target velocity angle provided by the outer control loop, and K_{c}, K_{f} are scalar gains to be chosen by the designer. We note that, with the proposed control design approach, K_{c} can be tuned in order to robustly stabilize the control loop, see [16], [17] for details.

C. Outer control loop

The outer control loop is responsible for providing the middle control loop with a reference heading $\gamma_{ref}(t)$. The goal is to have a control algorithm able to make the wing fly along figure-eight paths, without resorting to pre-computed trajectories to be used as reference, as it has been done in previous works [7], [10]. In fact, pre-computed reference paths are based on some mathematical model of the system, with the consequent unavoidable issues of model mismatch and approximation that might give rise to problems related to stability and attractiveness of the chosen trajectory. Moreover, a wind speed measurement would be needed in order to use the correct trajectory, and this is in general very hard to obtain. In [15], a bang-bang like strategy to set the reference heading of the wing, avoiding the use of pre-computed reference flying paths, has been described. Here, we propose an approach with a similar spirit, whose advantage is to provide an intuitive link between the tuning parameters and the position of the resulting paths in the wind window. In our approach we define two fixed reference points in the (ϕ, θ) plane, called $P_- = (\phi_-, \theta_-)$ and $P_+ = (\phi_+, \theta_+)$, with $\phi_- < \phi_+$ (see Fig. 5). The controller computes a new

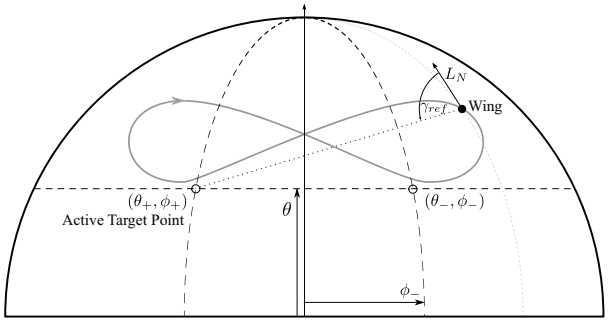

Fig. 5. Sketch of the control strategy for the outermost loop. Wind window projected on the (Y, Z) plane (black solid line), target points P_-, P_+ ('$\circ$'), traces of points with constant θ and ϕ (dashed lines), example of wing's path (gray solid line), and example of how the reference γ_{ref} is computed for a given wing position ('$\bullet$').

value of the reference velocity angle at discrete time instants. At each time step $k \in \mathbb{Z}$, one of the two reference points is set as the active target $P_{\text{a}}(k) = (\phi_{\text{a}}, \theta_{\text{a}})$, according to a switching strategy. Then, the reference velocity angle $\tilde{\gamma}_{\text{ref}}(k)$ is computed on the basis of the measured values of $\theta(k)$ and $\phi(k)$ in order to target the active reference point, see [16], [17] for details.

TABLE I

SYSTEM PARAMETERS

Name	Symbol	Value	Unit
Wing effective area	A	9	m^2
Wingspan	d_s	3.5	m
Distance between steering lines' attachment points	d	0.5	m
Tether length	r	30	m
Wing mass	m	2.45	kg
Air density	ρ	1.2	$\mathrm{kg/m}^3$

TABLE II

CONTROL PARAMETERS

Name	Symbol	Value	Unit
Low-level control loop damping	ζ_{cl}	0.7	–
Low-level control loop natural frequency	ω_{cl}	78	rad/s
Motor current saturation	$\bar{i}_{\mathrm{m}}$	10	A
Gain between δ_{m} and δ_{u}	$K_{\delta_{\mathrm{u}}}$	4	–
γ controller's feedback gain	K_{c}	0.046	m/rad
γ controller's feedforward gain	K_{f}	0.002	–
γ_{ref} lowpass filter cutoff frequency	ω_γ	0.25	Hz

IV. EXPERIMENTAL RESULTS

We implemented the controller described in section III on a real-time machine made by SpeedGoat® and programmed with the xPC Target® toolbox for MatLab®. The employed wing is a Airush® One 9 m^2 power kite. The sampling frequencies for the control loops are 100 Hz for the innermost controller and 50 Hz for the middle and outermost ones. A movie of the experimental tests is available online [22]. Tables I and II show the main system's parameters and controller's parameters, respectively. Fig. 6 shows an example of the courses of $\delta_{\mathrm{m,ref}}(t)$ and $\delta_{\mathrm{m}}(t)$ obtained during the experiments with the employed controller for the innermost control loop. The forces applied by the wing's lines on the actuator can be regarded to as an exogenous additive disturbance at this level. The effect of such disturbance can be clearly seen between points 2-3 and 6-7 in Fig. 6, where there is some error between the reference and actual position. By how the machine has been designed, the force exerted by each steering line on the actuator is equal to twice the force on the line. This amounts to approximately 800 N between points 2-3 and 6-7 in the figure. The tracking error induced by such disturbance does not influence much the performance of the overall system. The flown path corresponding to Fig. 6 can be seen in Fig. 7, as well as the line forces and the velocity angle of the wing. We chose the gain $K_{\mathrm{c}} = 0.046$ according to the robustness analysis presented in [17]. We remark that, due to the physical limitations of the actuator, the control input $\delta_{\mathrm{m,ref}}(t)$ is constrained in the range ± 0.35 m. This saturation was never active since, in practice, the commanded position was much lower, of the order of 0.1 m (see Fig. 6). Finally, we tuned the feedforward gain K_{f} through experiments, by gradually increasing it from 0, and set the value $K_{\mathrm{f}} = 0.002$. Such a small value is motivated by the fact that we chose not to cancel the geometric input (6), since its effect is to contribute to steer the wing towards the center of the wind-window, hence facilitating the desired up-loops figure eights.

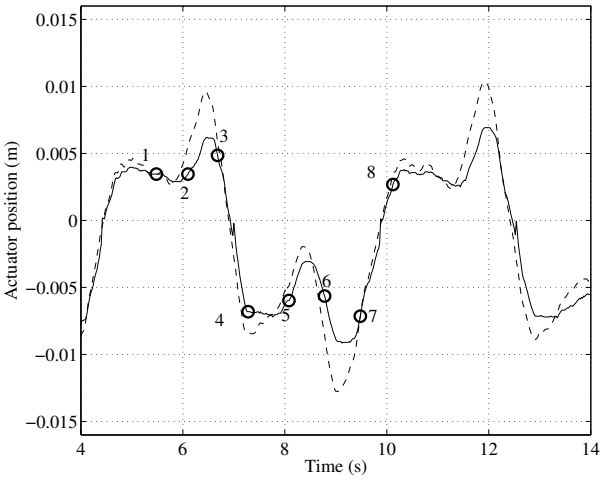

Fig. 6. Experimental results. Example of courses of target position $\delta_{\mathrm{m,ref}}(t)$ (dashed line) and actual position $\delta_{\mathrm{m}}(t)$ (solid line) of the actuator obtained with the designed innermost control loop, during automatic flight tests of a 9-m^2 wing. The numbered circles corresponds to the conditions highlighted in Fig. 7.

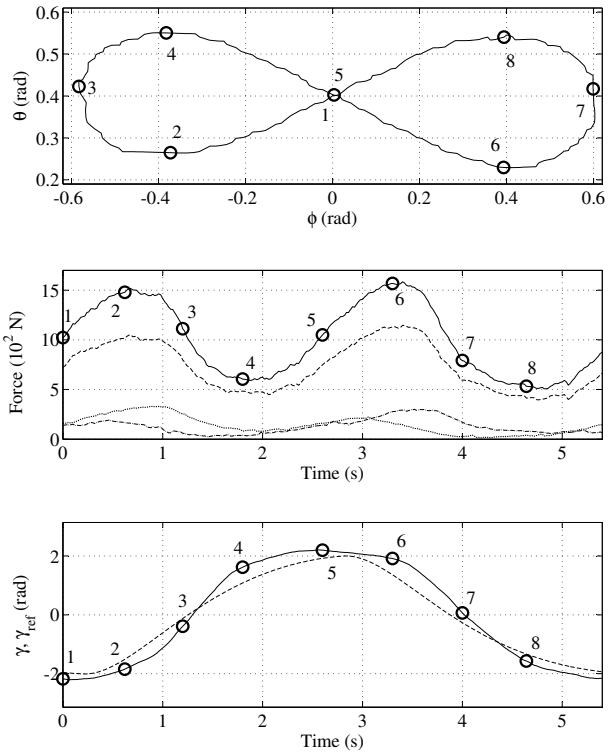

Fig. 7. Experimental results. Single figure-eight path obtained during automatic test flights with about 2.9 m/s wind speed. From top to bottom: flying path in (ϕ, θ) coordinates, course of the total force acting on the lines (solid line) and of the forces acting on the left (dotted), right (dash-dot) and center (dashed) lines, course of the velocity angle γ (solid line) and reference velocity angle γ_{ref} (dashed) .

In other words, the geometric input already gives place to a "self-steering" behavior, and the feedback controller applies relatively slight corrections to prevent instability and divergence of the flown paths, especially in the middle of the wind window where the geometric input is very small and the wing, without feedback control, would crash into the ground. This can be clearly seen by comparing the numbered points in Figs. 6 and 7 (top). On the bottom of Fig. 7, a typical example of the courses of the reference γ_{ref} and of the actual velocity angle γ obtained during the experiments can be seen: it can be noted that the middle control loop achieves good performance in tracking the desired velocity angle. The proposed control approach has been successfully tested under various conditions. The controller was able to deal with varying wind speed at ground level between about $2\,\mathrm{m/s}$ up to $6\,\mathrm{m/s}$, achieving similar, consistent flight paths also in the presence of gusts. Wind speeds lower than 2 m/s at ground level would not allow the employed wing to fly without stalling, and we avoided to test with wind speeds higher than 6 m/s at ground level not to stress too much the wing itself, the lines and the mechanical frame, pulleys and other components of the prototype (we recall that the involved forces increase linearly with the square of the wind speed). Misalignments of the GU with respect to the wind direction up to 30° did not pose a problem for the overall control strategy. However, if the target points (and thus the figure-eight paths) are not centered with respect to the wind, the flight trajectory becomes slightly asymmetric in terms of altitude. In Fig. 8, this phenomenon can be seen in the (ϕ, θ) plane. The forces are larger on one side of the loop and therefore the wing tends to gain more altitude during these turns. In Figs. 6-8, the target points' coordinates are

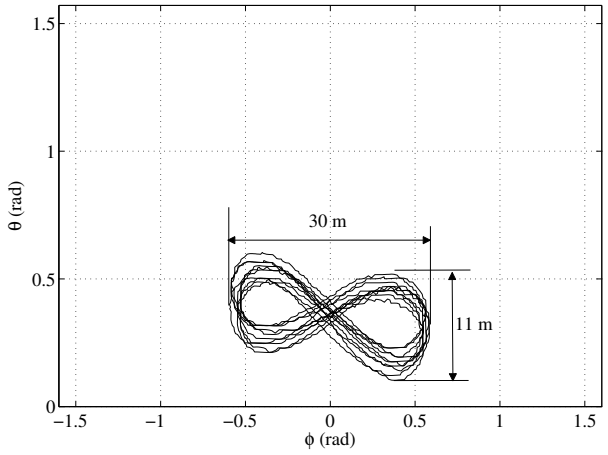

Fig. 8. Experimental results. Ten consecutive figure-eight paths in the (ϕ, θ) plane, and corresponding linear dimensions with the employed line length of 30 m. Thick solid line: trace of the wind window.

$$\theta_+ = \theta_- = 0.35,\ \phi_- = -0.2,\ \phi_+ = 0.2.$$

V. Conclusions

We described an approach to design a feedback controller for tethered wings to obtain figure-eight crosswind flying paths, to be used in airborne wind energy generators. The controller features three hierarchical levels. Differently from existing approaches in the literature, neither the measurement of the wind speed at the wing's altitude nor that of the effective wind speed are required. The control system involves few parameters, that can be easily tuned. We showed the effectiveness of the approach through experimental results obtained with a small scale prototype.

References

[1] Makani Power Inc., http://www.makanipower.com.

[2] SkySails GmbH & Co., 2010, http://www.skysails.info.

[3] Ampyx power website, http://www.ampyxpower.com/.

[4] Kitenergy website, http://www.kitenergy.net/.

[5] Swiss Kite Power collaborative research project, http://www.swisskitepower.ch/.

[6] M. Canale, L. Fagiano, and M. Milanese, "Power kites for wind energy generation," *IEEE Control Systems Magazine*, vol. 27, no. 6, pp. 25–38, December 2007.

[7] A. Ilzhöfer, B. Houska, and M. Diehl, "Nonlinear MPC of kites under varying wind conditions for a new class of large-scale wind power generators," *International Journal of Robust and Nonlinear Control*, vol. 17, pp. 1590–1599, 2007.

[8] M. Canale, L. Fagiano, and M. Milanese, "High altitude wind energy generation using controlled power kites," *IEEE Transactions on Control Systems Technology*, vol. 18, no. 2, pp. 279 –293, mar. 2010.

[9] E. Terink, J. Breukels, R. Schmehl, and W. Ockels, "Flight dynamics and stability of a tethered inflatable kiteplane," *AIAA Journal of Aircraft*, vol. 48, no. 2, pp. 503–513, 2011.

[10] J. H. Baayen and W. J. Ockels, "Tracking control with adaption of kites," *IET Control Theory and Applications*, vol. 6, no. 2, pp. 182–191, 2012.

[11] L. Fagiano and M. Milanese, "Airborne wind energy: an overview," in *American Control Conference 2012*, Montreal, Canada, 2012, pp. 3132–3143.

[12] M. L. Loyd, "Crosswind kite power," *Journal of Energy*, vol. 4, no. 3, pp. 106–111, 1980.

[13] P. Williams, B. Lansdorp, and W. Ockels, "Optimal crosswind towing and power generation with tethered kites," *Journal of guidance, control, and dynamics*, vol. 31, pp. 81–93, 2008.

[14] L. Fagiano, "Control of tethered airfoils for high–altitude wind energy generation," Ph.D. dissertation, Politecnico di Torino, Italy, February 2009, available on–line: http://lorenzofagiano.altervista.org/docs/PhD_thesis_Fagiano_Final.pdf.

[15] M. Erhard and H. Strauch, "Control of towing kites for seagoing vessels," *arXiv*, vol. abs/1202.3641, 2012.

[16] L. Fagiano, A. Zgraggen, M. Morari, and M. Khammash, "On control of tethered wings for airborne wind energy," in *American Control Conference 2013*, Washington DC, 17-19 June 2013.

[17] ——, "Automatic crosswind flight of tethered wings for airborne wind energy: modeling, control design and experimental results," *arXiv*, vol. 1301.1064, 2013, submitted to IEEE Trans. on Control Syst. Technology.

[18] L. Fagiano, K. Huynh, B. Bamieh, and M. Khammash, "Sensor fusion for tethered wings in airborne wind energy," in *American Control Conference 2013*, Washington DC, 17-19 June 2012.

[19] ——, "On sensor fusion for airborne wind energy systems," *arXiv*, vol. 1211.5060, 2012, submitted to IEEE Trans. on Control Syst. Technology.

[20] L. Fagiano, M. Milanese, and D. Piga, "High-altitude wind power generation," *IEEE Transactions on Energy Conversion*, vol. 25, no. 1, pp. 168 –180, mar. 2010.

[21] S. Skogestad and I. Postlethwaite, *Multivariable Feedback Control. 2^{nd} edition*. Wiley, 2005.

[22] EISG project "Autonomous flexible wings for high-altitude wind energy generation", experimental test movie, August 2012. Available on–line: http://lorenzofagiano.altervista.org/movies/EISG_UCSB_auto_wing.mp4.